Radiation Pressure Force from Optical Cycling on a Polyatomic Molecule

Ivan Kozyryev,[1,2,*] Louis Baum,[1,2] Kyle Matsuda,[1,2] Boerge Hemmerling,[1,2,3] and John M. Doyle[1,2]

[1]*Harvard-MIT Center for Ultracold Atoms, Cambridge, MA 02138, USA*
[2]*Department of Physics, Harvard University, Cambridge, MA 02138, USA*
[3]*Present address: Department of Physics, University of California, Berkeley, CA 94720, USA*

We demonstrate multiple photon cycling and radiative force deflection on the triatomic free radical strontium monohydroxide (SrOH). Optical cycling is achieved on SrOH in a cryogenic buffer-gas beam by employing the rotationally closed $P(N''=1)$ branch of the vibronic transition $\tilde{X}^2\Sigma^+(000) \leftrightarrow \tilde{A}^2\Pi_{1/2}(000)$. A single repumping laser excites the Sr-O stretching vibrational mode, and photon cycling of the molecule deflects the SrOH beam by an angle of 0.2° via scattering of ~ 100 photons per molecule. This approach can be used for direct laser cooling of SrOH and more complex, isoelectronic species.

I. INTRODUCTION

The use of laser radiation to control and cool external and internal degrees of freedom for neutral atoms [1], molecules [2, 3], microspheres [4, 5], and micromechanical membranes [6, 7] has revolutionized atomic, molecular, and optical physics. The powerful techniques of laser cooling and trapping using light scattering forces for atoms led to breakthroughs in both fundamental and applied sciences, including detailed studies of diverse degenerate quantum gases [8, 9], creation of novel frequency standards [10], precision measurements of fundamental constants [11, 12], and advances in quantum information processing [13, 14]. Beyond atoms, cold and ultracold molecules beckon with promising applications in controlled chemistry [15], many-body physics [16, 17], and quantum science [18, 19].

Following proposals by Di Rosa [20] and Stuhl et al. [21], as well as initial experimental results by Shuman et al. [22], laser cooling has been successfully applied to a few diatomic molecules (SrF [3], YO [23] and CaF [24]) and led to magneto-optical trapping of SrF at sub-millikelvin temperatures [25]. Recently, Isaev and Berger [26] identified promising polyatomic molecules for direct Doppler cooling based on Franck-Condon (FC) factor calculations. While a nonresonant dipole force was used to deflect a beam of CS_2 [27] and optical pumping led to rotational cooling of CH_3F [28], there has been no demonstration of the radiative force via optical cycling for a species with more than two atoms.

Polyatomic molecules are more difficult to manipulate than atoms and diatomic molecules because they possess additional constituents and their concomitant additional rotational and vibrational degrees of freedom. Partially because of their increased complexity, cold dense samples of molecules with three or more atoms offer unique capabilities for exploring interdisciplinary frontiers in physics, chemistry and even biology. Precise control over polyatomic molecules could lead to applications in astrophysics [29], quantum simulation [30] and computation [31], fundamental physics [32, 33], and chemistry [34]. Study of parity violation in biomolecular chirality [35] - which plays a fundamental role in molecular biology [36] - necessarily requires polyatomic molecules consisting of at least four atoms.

In recent years, a number of different experimental tools were developed for controlling neutral gas-phase polyatomic molecules, including Stark deceleration followed by electric trapping [37], pulsed magnetic slowing [38], buffer-gas cooling [39], rotating centrifugal slowing [40], and optical Stark deceleration [41]. However, with the exception of optoelectrical Sisyphus cooling [42, 43], the lowest temperatures reached were around 1 K [44]. While association of ultracold atoms into diatomic molecules has allowed creation of nearly degenerate bialkali molecular gases in the singlet ground state [45, 46], using similar methods to create more complex polyatomics appears challenging at the moment.

In this paper, we demonstrate optical cycling and the radiation pressure force on triatomic strontium monohydroxide (SrOH). The structure of SrOH is more complicated compared to previously laser cooled diatomic molecules: it contains three vibrational modes [47], including degenerate bending vibrations with no direct analog in diatomic molecules. Additionally, the Renner-Teller effect, which is absent in diatomics, further complicates molecular structure [48]. Our experimental results demonstrate that despite the significantly increased complexity associated with even a simple polyatomic molecule like SrOH, optical cycling on a quasi-closed transition can be applied with technically straightforward modifications. In particular, for this species (and those isoelectronic to it, to be discussed later in this paper), the additional degrees of freedom do not affect photon cycling up to the level of hundreds of photons, more than enough to implement deflection through radiative force. To reach the level of thousands of scattered photons (necessary to cool to the millikelvin regime), very similar techniques can be used, for example in SrOH by repumping the excited bending mode.

*Electronic address: ivan@cua.harvard.edu

II. EXPERIMENTAL DETAILS

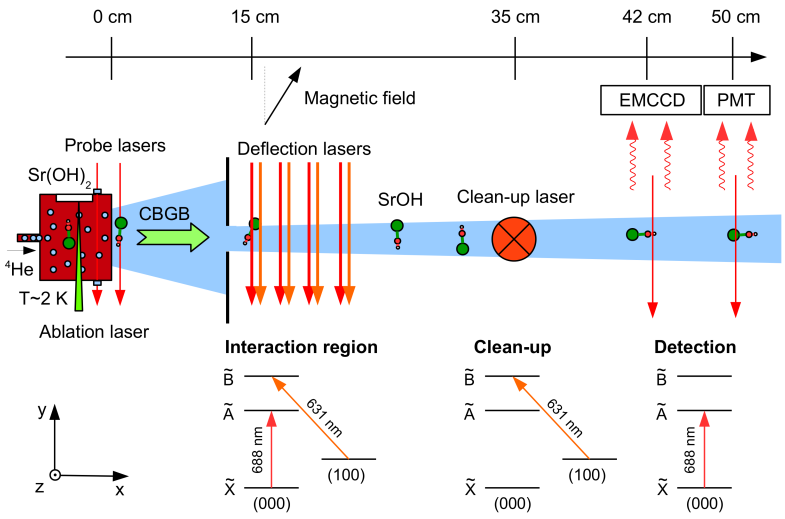

Figure 1: Schematic of the experimental setup (not to scale). A cryogenic beam of SrOH is produced using laser ablation of a pressed $Sr(OH)_2$ target followed by buffer-gas cooling with ~ 2 K helium gas. Transverse lasers, resonant with $P(N''=1)$ line of the $\tilde{X}^2\Sigma^+(000) \rightarrow \tilde{A}^2\Pi_{1/2}(000)$ and $\tilde{X}^2\Sigma^+(100) \rightarrow \tilde{B}^2\Sigma^+(000)$ electronic transitions, interact with the collimated molecular beam in order to apply radiation pressure force. In order to remix the dark magnetic sub-levels, a magnetic field at an angle of 60° is applied in the interaction region. Molecules remaining in the excited vibrational level of the electronic ground state are optically pumped back into the ground vibrational level using $\tilde{X} \rightarrow \tilde{B}$ off-diagonal excitation. The spatial profile of the molecular beam is imaged on the electron multiplying charge-coupled device (EMCCD) camera and the time-of-flight data is collected on the photomultiplier tube (PMT). The vibrational quantum numbers $(v_1v_2v_3)$ correspond to the Sr↔OH stretching (v_1), Sr-O-H bending (v_2), and SrO↔H stretching (v_3) vibrational modes.

A schematic diagram of the experimental apparatus is shown in figure 1. Gas-phase SrOH is produced by laser ablation of solid $Sr(OH)_2$ placed inside a cryogenic cell maintained at a temperature of ~ 2 K. The study of SrOH buffer-gas cooling dynamics, as well as measurements of its momentum transfer and inelastic cross sections with helium, were previously performed [49]. Detailed descriptions of the cryogenic and vacuum chambers used in this experiment have been provided elsewhere [50]. Briefly, SrOH molecules entrained in helium buffer gas flowing into the cell at a rate of 6 sccm (standard cubic centimeters per minute) are extracted into a beam through a 5 mm aperture. This cryogenic buffer-gas beam (CBGB) [51] contains approximately 10^9 molecules in the first excited rotational level ($N=1$) in a pulse about 5 ms long. The forward velocity of the SrOH beam is 130 ± 20 m/s and its transverse velocity spread is ± 15 m/s. A rectangular 2×2 mm slit situated 15 cm away from the cell aperture collimates the beam. Deflection of the molecules is achieved by applying laser light perpendicular to the beam's flight path. To increase the interaction time, several laser beams are applied in a series. The deflection laser beams originate from a single-mode fiber containing two colors - 688 nm for driving the $\tilde{X}^2\Sigma^+(000) \rightarrow \tilde{A}^2\Pi_{1/2}(000)$ transition and 631 nm for driving the $\tilde{X}^2\Sigma^+(100) \rightarrow \tilde{B}^2\Sigma^+(000)$ transition. The exact scheme is described in more detail in section III. Each color contains two frequency components separated by ~ 110 MHz to address $P_{11}(J''=1.5)$ and ${}^PQ_{12}(J''=0.5)$ lines of the spin-rotation (SR) splitting. Each dual-color beam has FWHM diameter of 1.8 mm and contains 50 mW of total laser power. In order to create multiple passes (to maximize molecule deflection), the same beam is circulated around the vacuum chamber. The light is generated using injection-locked laser diodes seeded by external-cavity diode lasers in the Littrow configuration [52]. In order to destabilize the dark states created during the cycling process [53], we apply a magnetic field of a few gauss at an angle of 60° to the polarization plane xz.

In the "clean-up" region, we repump all the molecular population from the excited vibrational level $\tilde{X}(100)$ back to the ground state in order to increase the signal in the detection region. The spatial profile of the molecular beam is extracted by imaging the laser-induced fluorescence (LIF) from a transverse retroreflected laser beam on an EMCCD camera. The laser beam addresses both SR components of the $P(N''=1)$ line for the $\tilde{X}^2\Sigma^+(000) \rightarrow \tilde{A}^2\Pi_{1/2}(000)$ transition with $\sim$ 1mW each. In a similar laser configuration, time-of-flight data is recorded by collecting the LIF on a PMT 8 cm downstream.

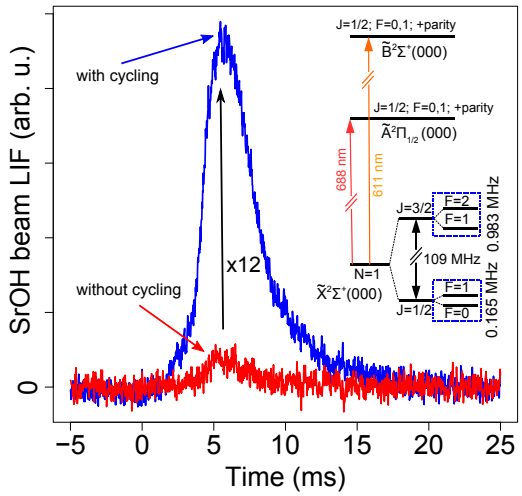

Figure 2: Laser induced fluorescence (LIF) increase due to photon cycling. The red trace shows the SrOH beam signal in the first excited rotational level ($N = 1$) when only one of the spin-rotation lines is addressed with the 688 nm laser resonant with the $P(N'' = 1)$ line of the $\tilde{X}^2\Sigma^+ \rightarrow \tilde{A}^2\Pi_{1/2}$ electronic transition. More than an order of magnitude LIF increase is observed (in blue) when two laser frequencies separated by ~ 110 MHz excite both of the spin-rotation lines. Increased fluorescence corresponds to the scattering of approximately 24 photons per each molecule limited by the decay to the dark vibrational level. The inset diagram shows relevant rotational, fine and hyperfine structure levels of SrOH. Rotationally closed excitations on the $\tilde{X} - \tilde{A}$ and $\tilde{X} - \tilde{B}$ electronic transition are shown with red and orange upward arrows, correspondingly. The unresolved hyperfine splittings (grouped in dashed squares) have previously been measured [54] and are smaller than the natural linewidth of the $\tilde{X} - \tilde{A}$ electronic transition [55].

III. RESULTS AND DISCUSSION

The rotationally closed electronic transitions used in this work are shown in the inset of figure 2. We chose the lowest frequency $\tilde{X} - \tilde{A}$ electronic excitation at 688 nm for optical cycling in the experiment because it can be addressed with all solid-state lasers. The diagonal FC factors of the $\tilde{X} - \tilde{A}$ band [49, 56] allow for scattering multiple photons before decaying to excited vibrational levels. Following a previously developed scheme for diatomics [22–24, 57], we address the molecules in the first excited rotational level on the $P(N'' = 1)$ line. Because of the rotational selection rules, molecules return to the same rotational state after the cycle $N'' = 1 \leftrightarrow N' = 0$. Hyperfine splittings in SrOH are below the natural linewidth of the electronic transition [54]. The observed fluorescence enhancement due to photon cycling is demonstrated in figure 2. The red trace shows the molecular beam signal without photon cycling when only the $P_{11}(J'' = 1.5)$ line is addressed and, therefore, on average, the molecules will scatter approximately two photons before decaying to the dark SR component. Adding the second laser frequency to excite the ${}^PQ_{12}(J'' = 0.5)$ transition, we see more than an order of magnitude increase in the LIF, which corresponds to about 24 scattered photons per molecule. We model the number of photon scattering events before a decay to the dark vibrational level $\tilde{X}(100)$ as a geometric distribution with probability of success p, identified as the "off-diagonal" FC factor $f_{\tilde{A}(000)\rightarrow\tilde{X}(100)}$. Since the expected value of the geometric probability distribution is $1/p$ [58], on average, $1/f_{\tilde{A}(000)\rightarrow\tilde{X}(100)} \approx 25$ photons are scattered per molecule before the loss to the dark vibrational level, which agrees with our observations. Figure 3 shows the scan of two laser frequencies together, where the spin-rotation components manifest themselves as peaks detuned by ~ 110 MHz from the center peak. The cycling LIF is larger than the combined signal for both of the SR components alone, indicating photon cycling in the molecular system.

The experimentally relevant vibrational structure of SrOH is depicted in the inset of figure 4. Upon electronic excitation, 96% of the molecules return to the vibrational ground state while 4% decay to the excited Sr-O stretching mode (100). We repump these molecules via the $\tilde{B}$ state using the 631 nm laser, as shown in the diagram. Figure 4 depicts cycling between the (000) and (100) vibrational levels of the ground electronic state $\tilde{X}$. By applying light in the interaction region, we pump all $\tilde{X}(000)$ molecules (in black) into the excited vibrational mode $\tilde{X}(100)$ after scattering of ~ 25 photons, which is indicated by the depleted beam profile (in red). Application of the repumping beam returns the molecules to the ground vibrational level and we recover the fluorescence signal (in blue). Cycling between vibrational levels indicates that the dominant vibrational loss mechanism in the molecular system is to the excited Sr-O stretching mode $\tilde{X}(100)$. It is estimated [49, 59] that the molecules will scatter about 1,000 photons before they decay to the second excited Sr-O stretching mode $\tilde{X}(200)$.

As previously mentioned in section I, in addition to Sr-O stretching, SrOH contains two other vibrational modes that can limit the photon cycling process. Because the vibrational angular momentum selection rule $\triangle l = 0$ allows only for specific decays to the excited bending mode vibrations from the $\tilde{A}(000)$ state [60], the dominant loss channel in the bending mode is to $\tilde{X}(02^00)$

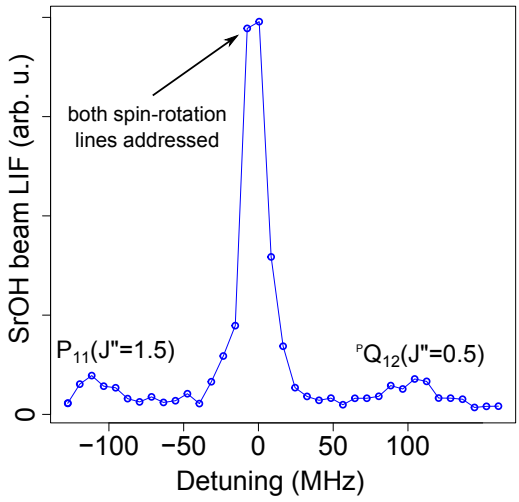

Figure 3: Fluorescence spectrum with photon cycling. A three-peak spectrum is observed upon scanning of two laser frequencies separated by ~ 110 MHz through the two spin-rotation components of the $P(N''=1)$ line for the $\tilde{X}^2\Sigma^+(000)-\tilde{A}^2\Pi_{1/2}(000)$ transition. Due to the photon cycling process, collected fluorescence with both spin-rotation lines addressed is an order of magnitude larger than the sum of the individual signals.

energy level with $l=0$. SrOH molecules will scatter at least 10,000 photons before decaying to the excited O-H stretching mode $\tilde{X}(001)$ [61]. Therefore, laser cooling can be effectively performed without the need for the O-H stretching mode repumping laser.

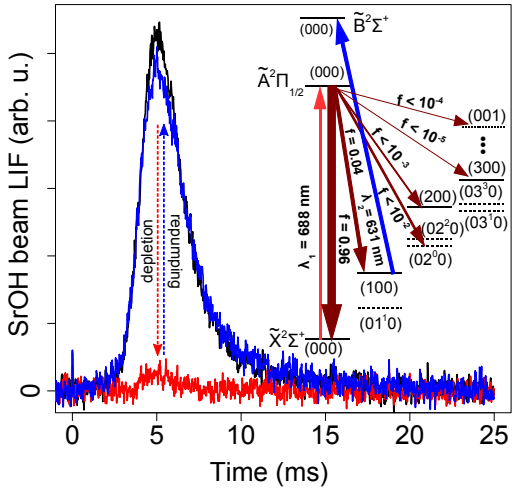

Figure 4: Cycling between vibrational levels. The molecular beam signal (black curve) is depleted (red curve) by the main cycling laser at 688 nm (light red, inset) due to off-diagonal vibrational decay to the excited vibrational mode (100). The signal is recovered (blue curve) by the application of the 631 nm repumping laser (blue, inset) in the clean-up region. The inset diagram shows the details of the vibrational structure of SrOH relevant to the optical cycling scheme. The energies of the excited vibrational levels in the electronic ground state have been previously measured [47]. The main cycling (λ_1) and repump (λ_2) lasers are indicated with the upward arrows, while the spontaneous decay channels in the Born-Oppenheimer approximation are shown with downward dark-red arrows. Thicker decay lines correspond to stronger transitions with the corresponding Franck-Condon factors (f) indicated. The values and bounds for FC factors are taken from [59]. The rotational states are not depicted at this scale. The superscript l next to the bending mode vibrational quantum number (v_2^l) indicates the projection of the vibrational angular momentum on the internuclear axis.

The effect of the radiation pressure force on SrOH due to photon cycling is shown in the deflection of the molecular beam (see figure 5). In order to extract the shift per photon in our setup, we perform cycling between (000) and (100) vibrational levels of the electronic ground state as described in figure 4. We measure the deflection with only the 688 nm laser applied in the interaction region and the 631 nm clean-up beam. We observe a shift of 0.007 mm/photon, which is consistent with the

value estimated from the travel distance and the forward velocity of the molecular beam. The measured deflection shown in figure 5(a) corresponds to about 90 scattered photons in the interaction region or 110 total scattered photons per molecule. From the comparison of the unnormalized signals scaled by the in-cell absorption (which indicates the total number of molecules produced), we determine that $\sim 20\%$ of the molecules are lost during the deflection process. Using a Bernoulli sequence to model the absorption-emission cycles [20], we estimate that the data indicate that the combined FC factor for loss to all dark vibrational levels is $(3 \pm 1) \times 10^{-3}$. Employing the Sharp-Rosenstock method [62], we calculate FC factors for decay from $\tilde{A}\,(000)$ to $\tilde{X}\,(200)$ and $\tilde{X}\,(02^0 0)$ to be $< 1 \times 10^{-3}$, but vibronic coupling and anharmonic terms in the potential could increase these decay rates [56, 63]. In particular, the large anharmonic contribution to the bending mode potential in SrOH [47] could lead to enhanced decay to the $\tilde{X}\,(02^0 0)$ state. The experimental efforts to precisely measure the FC factor for $\tilde{A}\,(000) \rightarrow \tilde{X}\,(02^0 0)$ are currently underway in our lab.

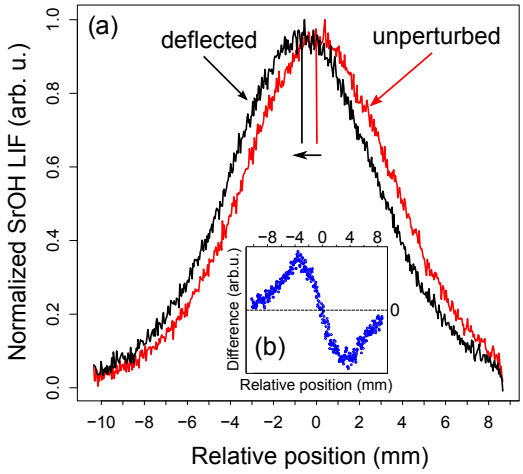

Figure 5: Deflection of the SrOH beam due to optical cycling. (a) Unperturbed spatial profile of the SrOH beam is shown in red. Upon the application of the transverse main and repump lasers in the interaction region the center of the beam distribution is shifted in the negative y direction (black curve). The shift of 0.65 mm between the centers of the peaks corresponds to the scattering of ~ 90 photons per molecule. (b) The measured difference between the normalized beam profiles vs position is shown. The deviation from zero (dashed black line) indicates the deflection of the molecular beam.

IV. CONCLUSIONS

By repumping out of only a single excited vibrational state, we demonstrated cycling of ~ 110 photons in SrOH. The ~ 90 photons absorbed in the interaction region lead to a 0.65 mm deflection of a cryogenic beam of SrOH. Our estimations indicate that the molecules lost from the photon cycle end up in the $\tilde{X}\,(02^0 0)$ excited bending mode. An additional repumping laser to pump the molecules out of the bending mode and back into the photon cycle would lead to scattering of $\sim 1{,}000$ photons per molecule, potentially allowing for laser cooling of SrOH to millikelvin temperatures [3]. Furthermore, the demonstrated optical cycling scheme opens a path towards the use of optical bichromatic forces [64–66] for rapid deceleration of SrOH originating from a CBGB [67] to near the capture velocity of a molecular MOT [57].

While SrOH has a linear geometry in the vibronic ground state, it also serves as a useful test candidate for the feasibility of laser cooling of more complex, nonlinear molecules. Other strontium monoalkoxide free radicals [68] look particularly promising for laser cooling applications. Our results corroborate previous observations that the $\tilde{X} \rightarrow \tilde{A}$ electronic transition in SrOH promotes a strontium-centered, nonbonding electron, leading to highly diagonal FC factors and the dominant vibrational activity associated with the Sr-O stretching mode [56, 69]. Thus, replacing the hydrogen atom with a more complex group R (e.g. CH_3 and CH_2CH_3) should not perturb the valence electron significantly [69]. SrO-R molecules share a number of properties with SrOH that are advantageous for laser cooling, including the previously mentioned very ionic Sr-O bond, linear local symmetry near the metal, diagonal Franck-Condon factors, and technically accessible laser transitions [69]. Further work in this vein should include the evaluation of FC factors for other vibrational modes and effects of Jahn-Teller coupling [60].

Acknowledgments

We would like to thank D. DeMille, J. Barry, T. Steimle, and P. Bernath for insightful discussions, as well as A. Sedlack for experimental contributions. This work was supported by the AFOSR.

---

[1] S. Chu, Rev. Mod. Phys. **70**, 685 (1998).
[2] M. Hamamda, P. Pillet, H. Lignier, and D. Comparat, J. Phys. B **48**, 182001 (2015).
[3] E. S. Shuman, J. F. Barry, and D. DeMille, Nature **467**, 820 (2010).
[4] N. Kiesel, F. Blaser, U. Delić, D. Grass, R. Kaltenbaek, and M. Aspelmeyer, Proc. Natl. Acad. Sci. U.S.A. **110**, 14180 (2013).
[5] P. Asenbaum, S. Kuhn, S. Nimmrichter, U. Sezer, and M. Arndt, Nat. Comm. **4** (2013).
[6] R. Peterson, T. Purdy, N. Kampel, R. Andrews, P.-L. Yu, K. Lehnert, and C. Regal, Phys. Rev. Lett. **116**, 063601 (2016).
[7] J. Chan, T. M. Alegre, A. H. Safavi-Naeini, J. T. Hill, A. Krause, S. Gröblacher, M. Aspelmeyer, and O. Painter, Nature **478**, 89 (2011).
[8] D. Greif, M. F. Parsons, A. Mazurenko, C. S. Chiu, S. Blatt, F. Huber, G. Ji, and M. Greiner, Science **351**, 953 (2016).
[9] W. S. Bakr, A. Peng, M. E. Tai, R. Ma, J. Simon, J. I. Gillen, S. Foelling, L. Pollet, and M. Greiner, Science **329**, 547 (2010).
[10] A. D. Ludlow, M. M. Boyd, J. Ye, E. Peik, and P. O. Schmidt, Rev. Mod. Phys. **87**, 637 (2015).
[11] J. B. Fixler, G. Foster, J. McGuirk, and M. Kasevich, Science **315**, 74 (2007).
[12] P. Cladé, E. De Mirandes, M. Cadoret, S. Guellati-Khélifa, C. Schwob, F. Nez, L. Julien, and F. Biraben, Phys. Rev. Lett. **96**, 033001 (2006).
[13] K. Maller, M. Lichtman, T. Xia, Y. Sun, M. Piotrowicz, A. Carr, L. Isenhower, and M. Saffman, Phys. Rev. A **92**, 022336 (2015).
[14] P. Jessen, I. Deutsch, and R. Stock, Quantum Inf. Process. **3**, 91 (2004).
[15] R. V. Krems, Phys. Chem. Chem. Phys. **10**, 4079 (2008).
[16] L. D. Carr, D. DeMille, R. V. Krems, and J. Ye, New J. Phys. **11**, 055049 (2009).
[17] D.-W. Wang, M. D. Lukin, and E. Demler, Phys. Rev. Lett. **97**, 180413 (2006).
[18] A. André, D. DeMille, J. M. Doyle, M. D. Lukin, S. E. Maxwell, P. Rabl, R. J. Schoelkopf, and P. Zoller, Nature Phys. **2**, 636 (2006).
[19] P. Rabl, D. DeMille, J. Doyle, M. Lukin, R. Schoelkopf, and P. Zoller, Phys. Rev. Lett. **97**, 033003 (2006).
[20] M. Di Rosa, Eur. Phys. J. D **31**, 395 (2004).
[21] B. K. Stuhl, B. C. Sawyer, D. Wang, and J. Ye, Phys. Rev. Lett. **101**, 243002 (2008).
[22] E. S. Shuman, J. F. Barry, D. R. Glenn, and D. DeMille, Phys. Rev. Lett. **103**, 223001 (2009).
[23] M. T. Hummon, M. Yeo, B. K. Stuhl, A. L. Collopy, Y. Xia, and J. Ye, Phys. Rev. Lett. **110**, 143001 (2013).
[24] V. Zhelyazkova, A. Cournol, T. E. Wall, A. Matsushima, J. J. Hudson, E. Hinds, M. Tarbutt, and B. Sauer, Phys. Rev. A **89**, 053416 (2014).
[25] E. Norrgard, D. McCarron, M. Steinecker, M. Tarbutt, and D. DeMille, Phys. Rev. Lett. **116**, 063004 (2016).
[26] T. Isaev and R. Berger, Phys. Rev. Lett. **116**, 063006 (2016).
[27] H. Stapelfeldt, H. Sakai, E. Constant, and P. B. Corkum, Phys. Rev. Lett. **79**, 2787 (1997).
[28] R. Glöckner, A. Prehn, B. G. Englert, G. Rempe, and M. Zeppenfeld, Phys. Rev. Lett. **115**, 233001 (2015).
[29] E. Herbst and E. F. Van Dishoeck, Annu. Rev. Astron. Astrophys. **47**, 427 (2009).
[30] M. Wall, K. Maeda, and L. D. Carr, New J. Phys. **17**, 025001 (2015).
[31] C. M. Tesch and R. de Vivie-Riedle, Phys. Rev. Lett. **89**, 157901 (2002).
[32] M. Kozlov, Phys. Rev. A **87**, 032104 (2013).
[33] M. G. Kozlov and S. A. Levshakov, Ann. Phys. (Berlin) **525**, 452 (2013).
[34] H. Sabbah, L. Biennier, I. R. Sims, Y. Georgievskii, S. J. Klippenstein, and I. W. Smith, Science **317**, 102 (2007).
[35] M. Quack, J. Stohner, and M. Willeke, Annu. Rev. Phys. Chem. **59**, 741 (2008).
[36] M. Quack, Angew. Chem. Int. Ed. **41**, 4618 (2002).
[37] H. L. Bethlem, G. Berden, F. M. Crompvoets, R. T. Jongma, A. J. Van Roij, and G. Meijer, Nature **406**, 491 (2000).
[38] T. Momose, Y. Liu, S. Zhou, P. Djuricanin, and D. Carty, Phys. Chem. Chem. Phys. **15**, 1772 (2013).
[39] D. Patterson and J. M. Doyle, Phys. Chem. Chem. Phys. **17**, 5372 (2015).
[40] S. Chervenkov, X. Wu, J. Bayerl, A. Rohlfes, T. Gantner, M. Zeppenfeld, and G. Rempe, Phys. Rev. Lett. **112**, 013001 (2014).
[41] R. Fulton, A. I. Bishop, and P. F. Barker, Phys. Rev. Lett. **93**, 243004 (2004).
[42] M. Zeppenfeld, B. G. U. Englert, R. Glöckner, A. Prehn, M. Mielenz, C. Sommer, L. D. van Buuren, M. Motsch, and G. Rempe, Nature **491**, 570 (2012).
[43] A. Prehn, M. Ibrügger, R. Glöckner, G. Rempe, and M. Zeppenfeld, Phys. Rev. Lett. **116**, 063005 (2016).
[44] M. Lemeshko, R. V. Krems, J. M. Doyle, and S. Kais, Mol. Phys. **111**, 1648 (2013).
[45] K.-K. Ni, S. Ospelkaus, M. De Miranda, A. Pe'er, B. Neyenhuis, J. Zirbel, S. Kotochigova, P. Julienne, D. Jin, and J. Ye, Science **322**, 231 (2008).
[46] J. W. Park, S. A. Will, and M. W. Zwierlein, Phys. Rev. Lett. **114**, 205302 (2015).
[47] P. I. Presunka and J. A. Coxon, Chem. Phys. **190**, 97 (1995).
[48] J. M. Brown and F. Jørgensen, Adv. Chem. Phys. **52**, 117 (1983).
[49] I. Kozyryev, L. Baum, K. Matsuda, P. Olson, B. Hemmerling, and J. M. Doyle, New J. Phys. **17**, 045003 (2015).
[50] B. Hemmerling, G. K. Drayna, E. Chae, A. Ravi, and J. M. Doyle, New J. Phys. **16**, 063070 (2014).
[51] N. R. Hutzler, H.-I. Lu, and J. M. Doyle, Chem. Rev. **112**, 4803 (2012).

[52] Y. Cunyun, *Tunable external cavity diode lasers* (Hackensack: World Scientific, 2004).
[53] D. Berkeland and M. Boshier, Phys. Rev. A **65**, 033413 (2002).
[54] D. Fletcher, K. Jung, C. Scurlock, and T. Steimle, J. Chem. Phys. **98**, 1837 (1993).
[55] J. Nakagawa, R. F. Wormsbecher, and D. O. Harris, J. Mol. Spectrosc. **97**, 37 (1983).
[56] C. Brazier and P. Bernath, J. Mol. Spectrosc. **114**, 163 (1985).
[57] B. Hemmerling, E. Chae, A. Ravi, L. Anderegg, G. K. Drayna, N. R. Hutzler, A. L. Collopy, J. Ye, W. Ketterle, and J. M. Doyle, arXiv:1603.02787 [physics.atom-ph] (2016).
[58] J. Rice, *Mathematical statistics and data analysis* (Belmont: Thomson Higher Education, 2010), 3rd ed.
[59] T. Nguyen, D. L. Kokkin, T. Steimle, I. Kozyryev, and J. M. Doyle, in *International Symposium on Molecular Spectroscopy* (2015).
[60] G. Herzberg, *Molecular spectra and molecular structure. Vol. 3: Electronic spectra and electronic structure of polyatomic molecules*, vol. 3 (New York: Van Nostrand, 1966).
[61] M. D. Oberlander, Ph.D. thesis, Ohio State University (1995).
[62] T. Sharp and H. Rosenstock, J. Chem. Phys. **41**, 3453 (1964).
[63] G. Fischer, *Vibronic coupling: The interaction between the electronic and nuclear motions* (New York: Academic Press, 1984).
[64] M. Chieda and E. Eyler, Phys. Rev. A **84**, 063401 (2011).
[65] L. Aldridge, S. Galica, and E. Eyler, Phys. Rev. A **93**, 013419 (2016).
[66] S. Galica, L. Aldridge, and E. Eyler, Phys. Rev. A **88**, 043418 (2013).
[67] H.-I. Lu, J. Rasmussen, M. J. Wright, D. Patterson, and J. M. Doyle, Phys. Chem. Chem. Phys. **13**, 18986 (2011).
[68] P. F. Bernath, Adv. Photochem. **23**, 1 (1997).
[69] C. Brazier, L. Ellingboe, S. Kinsey-Nielsen, and P. Bernath, J. Am. Chem. Soc. **108**, 2126 (1986).